J Mol Model (2004) 10:373–381
DOI 10.1007/s00894-004-0205-x

ORIGINAL PAPER

Xianfeng Chen · Irene T. Weber · Robert W. Harrison

Molecular dynamics simulations of 14 HIV protease mutants in complexes with indinavir

Received: 26 March 2004 / Accepted: 7 July 2004 / Published online: 28 September 2004
© Springer-Verlag 2004

Abstract The molecular mechanisms of HIV drug resistance were studied using molecular dynamics simulations of HIV-1 protease complexes with the clinical inhibitor indinavir. One nanosecond molecular dynamics simulations were run for solvated complexes of indinavir with wild type protease, a control variant and 12 drug resistant mutants. The quality of the simulations was assessed by comparison with crystallographic and inhibition data. Molecular mechanisms that contribute to drug resistance include structural stability and affinity for inhibitor. The mutants showed a range of structural variation from 70 to 140% of the wild type protease. The protease affinity for indinavir was estimated by calculating the averaged molecular mechanics interaction energy. A correlation coefficient of 0.96 was obtained with observed inhibition constants for wild type and four mutants. Based on this good agreement, the trends in binding were predicted for the other mutants and discussed in relation to the clinical data for indinavir resistance.

Keywords Drug resistance · Aspartic protease · Structural flexibility · Inhibition · Interaction energy

X. Chen · R. W. Harrison
Department of Biology, Molecular Basis of Disease Program,
Georgia State University,
Atlanta, GA 30303, USA

R. W. Harrison
Department of Computer Science,
Molecular Basis of Disease Program,
Georgia State University,
Atlanta, GA 30303, USA

I. T. Weber (✉)
Department of Biology,
Georgia State University,
P.O. Box 4010, Atlanta, GA 30302-4010, USA
e-mail: iweber@gsu.edu
Tel.: +1 404 651-0098
Fax: +1 404 651-2509

Introduction

Long-term anti-retroviral therapy for AIDS using protease inhibitors is compromised by the rapid selection of drug resistant mutants of the protease. Clinical isolates show extensive protease mutations that confer cross-resistance and multi-drug resistance to protease inhibitors. [1, 2, 3] Even in the absence of anti-retroviral drugs HIV is genetically diverse, especially in the protease gene that showed variations in up to 50 different residues. [4] One of the first protease inhibitors in clinical use was indinavir. Resistance to indinavir arises by a combination of several different mutations in the protease gene. [5] High levels of resistance are thought to require substitutions of up to 11 residues in the protease, although many different combinations have been observed. [6] No single combination predominates in clinical isolates. [7] Mutations of conserved residues M46 and V82 are the most common with indinavir treatment, followed by mutations of I54, L90, L24, G73, V32, I84, G48, and F53 at lower frequencies. Other protease inhibitors show a different pattern of resistant mutations. [8] Due to this complexity HIV genotyping has been recommended in clinical treatment of AIDS and knowledge-based expert systems are being developed to interpret the mutation data. [9] Knowledge-based expert systems interpolate or extract features from existing data and do not necessarily reflect the underlying chemical and physical basis for the drug resistant phenotype. Therefore, in parallel with those studies, it is important to analyze the molecular changes due to the resistant mutations in order to develop better antiviral therapies.

The clinical protease inhibitors, including indinavir, were a success of structure-based design, and numerous crystal structures are available for wild type protease with a variety of inhibitors. [10] Protease mutations observed in drug resistance have been classified as substitutions in the active site (or inhibitor binding site), the flexible flaps, or other non-active site residues. Earlier studies emphasized the effect of mutation of the active site residues. Reduced inhibition was observed for 10–11 different

mutants of active site residues that can directly alter interactions with indinavir. [11, 12] Local structural changes were associated with substitutions of V82 and I84 in the indinavir binding site. [13, 14] Recently, the non-active site substitutions were shown to have a significant effect on inhibitor affinity. [15, 16] Cooperative effects on inhibition were observed between active site and distal mutations. [17] However, structural and inhibition data are scarce, particularly for many of the non-active site mutations.

Molecular mechanics and dynamics simulations can be used to predict the effects of mutations on the protease structure and binding of inhibitor. Molecular dynamics simulations of HIV protease have been used to evaluate the catalytic mechanism, [18, 19, 20] the structural flexibility, [21, 22, 23] and the contribution of individual residues to binding of substrate and inhibitor. [24] Previously, we compared molecular mechanics interaction energies with the relative order of inhibition of indinavir by wild type protease and eight mutants. [25] These calculations used a single conformation of the protease–inhibitor complex with a screening term to more correctly reproduce the electron distribution of atoms. The best indinavir model gave a correlation coefficient of 0.68 between the calculated interaction energies and free energies from inhibition constants for all nine models. Here, molecular dynamics simulations of solvated complexes of 13 protease mutants with indinavir were run in order to better model the solution behavior without the screening term and to evaluate the physical basis for drug resistance.

Materials and methods

Selection of resistant mutations

A relational database [7] was searched for protease sequences in HIV isolates that were observed on exposure to indinavir as the only protease inhibitor. The proteases sequences were sorted using AWK scripts to obtain the frequencies of occurrence of different combinations of substitutions. Mutations L24I, V32I, K45I, M46I, M46L, G48V, F53L, I54V, G73S, V82A, I84V, N88D and L90M were selected. Mutant K45I is rare in clinical isolates, however, it was chosen as an example with increased activity, stability and a high resolution crystal structure. [26]

Molecular dynamics simulations

The 1.5-Å resolution crystal structure of HIV protease K45I mutant (PDB entry 1DAZ [26]) was combined with indinavir as the starting model, as described previously. [25] Models were made of wild type (WT) protease and proteases with 13 single substitutions representing resistant variants. The program AMMP [27] was used with the all-atom sp4 potential set. [28, 29] The charge generation parameters were taken from Bagossi et al. (1999). [30] The new atoms were built using the Kohonen and analytic model building features of AMMP, [31] and minimized with conjugate gradients. The partial charges for the inhibitor atoms were generated by a method of moments calculation, as described for the tetrahedral reaction intermediate of HIV protease. [28] Indinavir was modeled with positive charges on the N1 and N3 atoms and included a sulfate ion with ionic interactions with both N3 of indinavir and the side chain nitrogen atoms of Arg 8. [25] No screening dielectric term or bulk solvent correction was included. A constant dielectric of one was used. The amortized fast multipole algorithm in AMMP was used for the long range terms in the non-bonded and electrostatic potentials so that no-cutoff radius was employed. [32]

The 1994 waters were placed randomly to be self-avoiding and formed a 10-Å minimum shell around the wild type model of the indinavir complex. The initial distribution of waters was then energy minimized with protein and inhibitor atoms fixed, followed by 10 ps of molecular dynamics to establish a stable starting structure. The volume of the system was constrained to 179,594 $Å^3$ and the temperature was constrained to 300 K using Nose constraints as described in [18, 27]. Therefore, these simulations were in a constant NVT ensemble corresponding to a pressure of about 1 atm. The starting models for the mutants were generated from this initial model by changing only the side chain atoms of the mutated residues. The new residues were built by energy minimization with the rest of the atoms constrained to fixed locations. Thus the wild type and each mutant protease started from what was essentially the same point.

Analysis of simulations

1,000 frames, one for each picosecond, were saved from each 1-ns molecular dynamics (MD) run. The average interaction energy or total external non-bonded energy was calculated over the 1-ns run for indinavir in the protease complex. The protease structures were superimposed and Poincare maps calculated as described in [18]. The Poincare representations of the probability density of the atoms for each simulation were displayed like crystallographic electron density maps using the molecular graphics program O. [33] The mean and variance (σ^2) of the atomic positions were calculated and the average temperature factor (B) calculated from $8\pi\sigma^2$ for each residue in the protease and over each 1-ns simulation. The mode structures were calculated over the 1-ns simulation and examined using RasMol. [34]

Results

HIV protease mutations were selected after analysis of protease sequences from clinical isolates. There was no predominant combination of mutations in clinical isolates after indinavir treatment. [7] In fact, no specific combination was observed in more than 2% of the isolates. Therefore, the 12 mutations L24I, V32I, G48V, M46I, M46L, F53L, I54V, G73S, V82A, I84V, and L90M were chosen to reflect the range of single substitutions contributing to resistance to indinavir. N88D is uncommon on exposure to indinavir, but it is frequently observed on exposure to a different inhibitor, nelfinavir. [8] K45I is rare in clinical isolates; however, this mutant was selected since it shows higher stability and catalytic activity than the wild type protease and has proved valuable for comparison. [26] The locations of these mutations in the structure of HIV protease dimer with indinavir are shown in Fig. 1. The mutants include substitutions of residues in the indinavir binding site (V32I, V82A and I84V), the flaps (K45I, M46L, G48V, F53L and I54V), and non-active site regions (L24I, G73S, N88D, and L90M). Models were built for the WT protease and these 13 protease mutants in their complexes with indinavir and MD simulations run for 1 ns on the solvated complexes. The MD simulations were analyzed to reveal differences

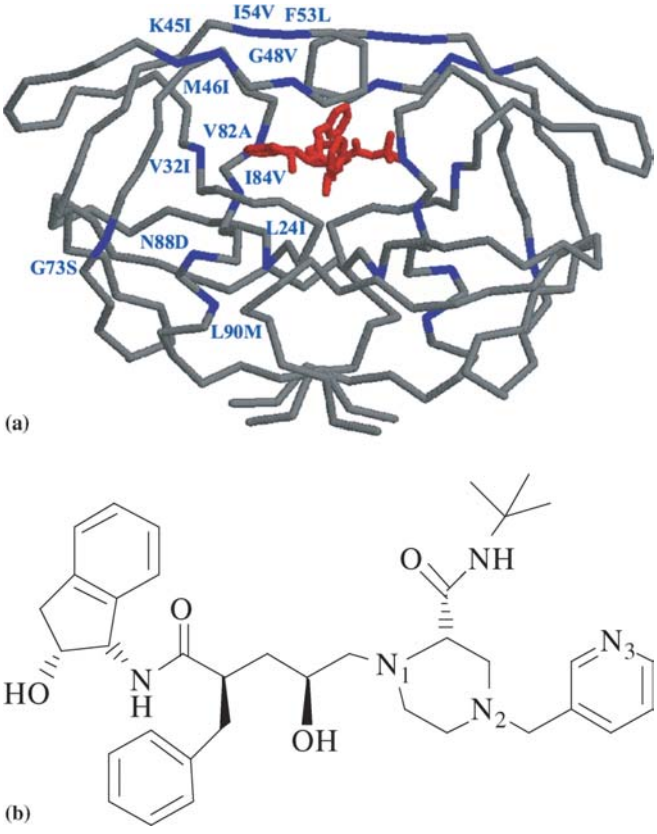

Fig. 1 a Location of mutations on HIV protease dimer structure. The mutations are labeled in *blue* on the alpha carbon backbone of one subunit of the HIV protease dimer. Indinavir is shown in *red*. **b** Structure of indinavir

in structure, flexibility, and interactions with indinavir that can lead to resistance.

Overall structural variation

The protease–indinavir complexes rapidly reached a stable equilibrium within 50 ps of dynamics. Subsequently, the root mean square difference (RMSD) of the alpha carbon atoms varied between 0.5 and 1.1 Å from the mean position over the 1-ns simulation. Other groups have reported similar results for nanosecond simulations on HIV protease. [23] These values are comparable to differences observed between HIV protease crystal structures, since analysis of 73 crystal structures of HIV protease–inhibitor complexes showed an average RMSD of 0.56 Å for main chain atoms. [35]

The structural variations were assessed by calculating the temperature factors over the simulations. The temperature factor per residue varied along the polypeptide chain in a similar manner for all simulations, as shown for WT protease in Fig. 2a. Both subunits in the dimer showed similar variations. The regions of low variation in all complexes were residues 5, 22–28, 31–33, 64, 71, and 84–91 in both subunits. The most stable region includes the catalytic Asp 25 and residues 23, 27–30 and 32 in the inhibitor binding site. The C-terminal stable region includes 84 in the inhibitor binding site, and residues near the C-terminus that form intersubunit interactions. The largest variation is observed for surface turn around residues 16–18, the surface loop from 34–43, and flap residues 44–57 of both subunits. Only the flap mutations were located in a variable region. The variation of the calculated temperature factor is very similar to the observed variation in RMSD values for main chain atoms averaged over 73 crystal structures of protease–inhibitor complexes. [35] Therefore, the MD simulations reflected the observed positional variations in the protease crystal structures.

The average atomic temperature factor was calculated for each MD trajectory as a measure of the overall positional variation. The overall values ranged from 21.1 to 40.3 $Å^2$, as shown in Fig. 2b. These values were comparable to values from crystal structures. For example, the first crystal structure of HIV protease with indinavir (1HSG [36]) had an average atomic temperature factor of 31.0 $Å^2$. The wild type protease, and the majority of mutants showed values in the range of 26–31 $Å^2$. The mutants, K45I and M46I in the flap and non-active site L24I, showed substantially lower calculated temperature factors of 21–23 Å. V32I in the indinavir binding site showed the highest value of 40.3 $Å^2$. Therefore, the overall structural variation appeared to be independent of the location of the mutated residue relative to the indinavir binding site.

Positional variation of individual atoms in protease–indinavir complexes

The positional variation of individual atoms over the 1,000 frames was analyzed by calculating the Poincare maps, as described previously. [18] The Poincare map shows the mode of the atomic positions and is not biased by large atomic variations that are rare events in the simulations, unlike the calculated temperature factor or RMSD values. The Poincare maps showed clear representation of all the protease residues in all models. The protein atoms, including hydrogen atoms, were clearly defined as shown for Tyr 59 in the simulation for WT protease (Fig. 3a). The hydrogen atoms of methyl rotors were generally in well-defined positions, as shown for Thr 31 in the WT simulation (Fig. 3b). Most of the indinavir atoms, including the hydrogens, were clearly represented in all simulations. The benzyl group of indinavir from the WT complex is shown in Fig. 3c. One exception was the pyridyl group, which was clearly represented in the complexes with mutants V32I, F53L, I84V, and N88D, but disordered in the other complexes. This disorder is not surprising, since the pyridyl group is partly exposed to solvent at the protein surface, and has been observed in different positions in protease–indinavir crystal structures. [37] The indinyl group showed partial disorder in the complexes with G73S, V82A, and I84V. Some of the solvent molecules that are observed in the crystal struc-

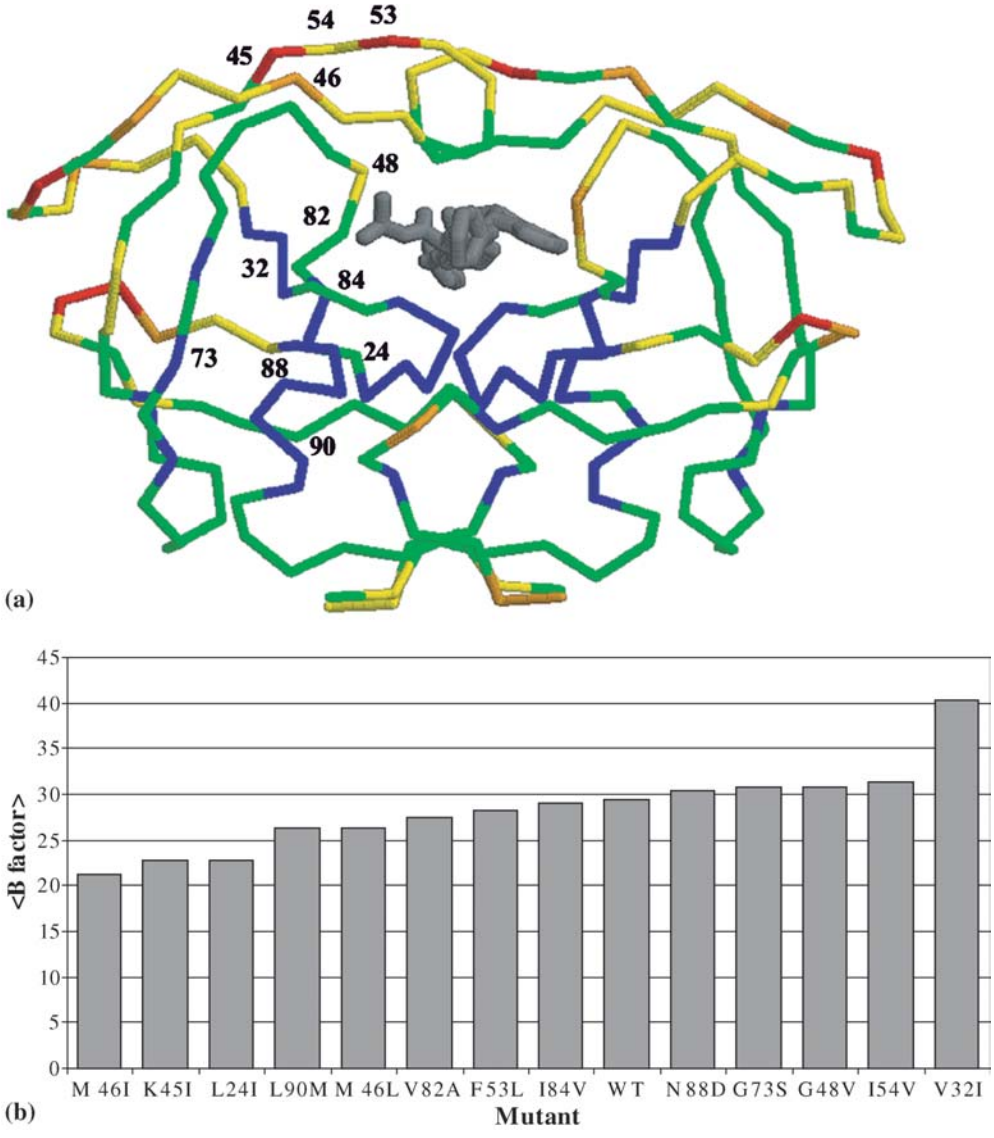

Fig. 2a, b Temperature factor analysis. **a** Alpha carbon backbone of WT protease is colored by the average *B*-factor per residue (A^2). *Red*, *B*>90.0; *orange*, 90.0>*B*>60.0; *yellow*, 60.0>*B*>30.0; *green*, 30.0>*B*>10.0; *blue*, 10.0>*B*>0.0. The sites of mutations are labeled. Indinavir is in *gray*. **b** Average *B*-factor (A^2) for each complex

tures were also conserved in the Poincare density maps. Interestingly, two conserved water molecules formed a network of hydrogen bond interactions connecting Thr 26, Gly 27, Asp 29, Arg 87, and indinavir (Fig. 3d). A similar network of interactions was observed in the crystal structure of HIV protease with indinavir. [36] Therefore, the average atomic positions for protease, indinavir, and some solvent atoms in the simulations were consistent with the crystal structures.

Comparison of average structures

The mode structures were compared for the mutants and the WT protease (Fig. 4a). The majority of mutants showed overall differences in the range of 0.8–1.1 Å for main chain atoms (Table 1). Only mutants I54V and V32I showed RMSD values of more than 1.2 Å for main chain atoms. These two mutants had also shown the greatest variation in atomic position (Fig. 2b). Although I54V alters a residue in the flexible flaps, the other flap mutants F53L, K45I, M46I, M46L and G48V were more similar to the WT structure.

The RMSD values for main chain atoms were analyzed as shown for the mutants L24I, I54V, and F53L in Fig. 4b. In general, the differences follow a pattern similar to that of the *B*-factor plot (Fig. 2a). Low differences of less than 1.0 Å were observed for main chain atoms of residues 9–13, 23–33, 82–92, 9'–13', 20'–33', and 84'–97' for most of the averaged structures (Fig. 4a). Larger differences occurred at the termini, near the surface turn of residues 16–18, surface residues 35–40, the flap residues 45–55, the surface turn of 67–69, and 79–83 in both subunits of the dimer. Different crystal structures showed more variability in those regions. [35]

The regions that interact directly with inhibitor were examined for larger differences (Table 1). RMSD values of >1.0 Å were considered significant in the least variable region of 21–31 that contains the catalytic residues. Differences of >2.0 Å were considered to be more significant

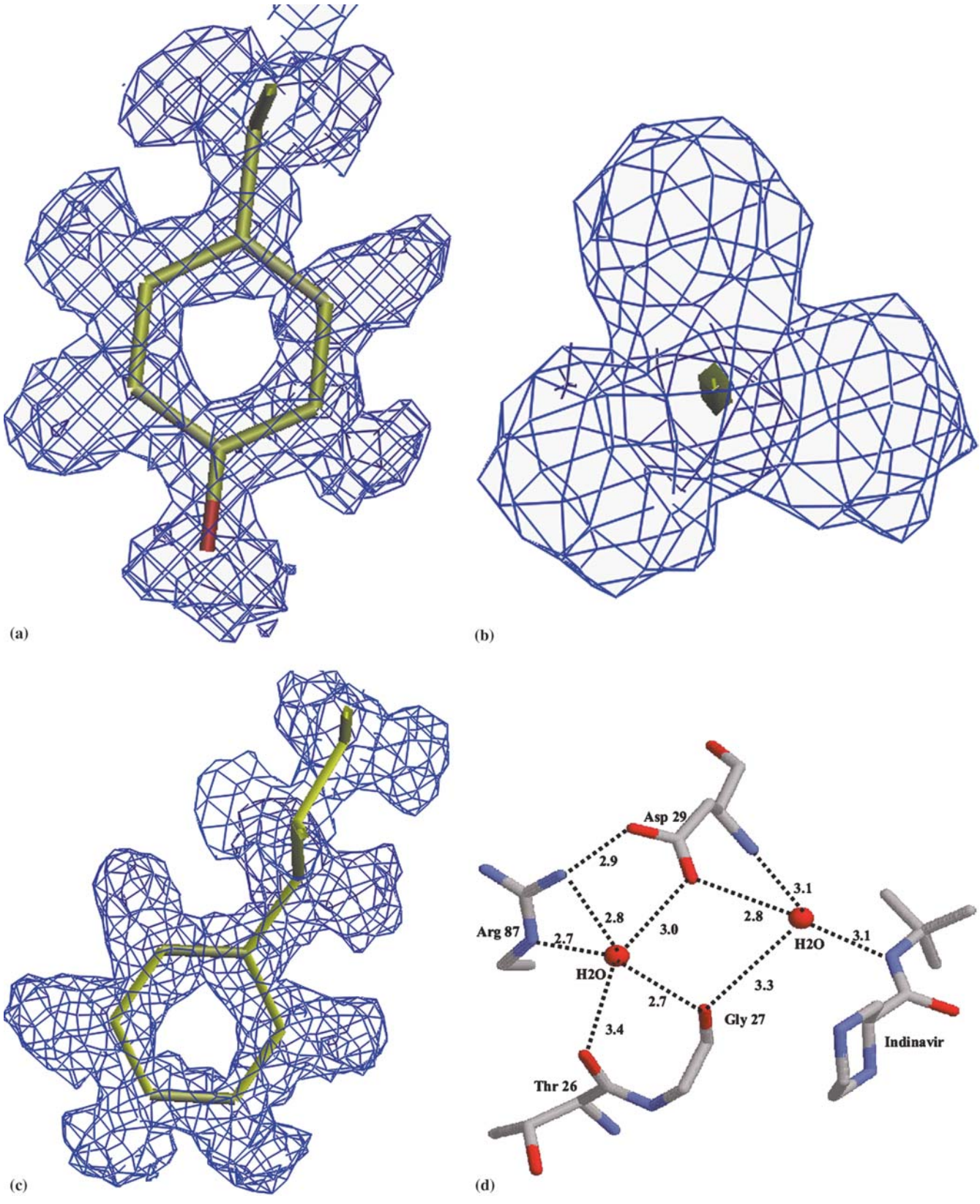

Fig. 3a–d Poincare map representation for WT protease–indinavir complex. **a** The side chain of Tyr 59 showing the positions of hydrogen atoms. **b** Methyl group of CG in Thr 31. View looking down the CG to CB bond. **c** Benzyl group of indinavir. **d** Two conserved water molecules and their hydrogen bond interactions

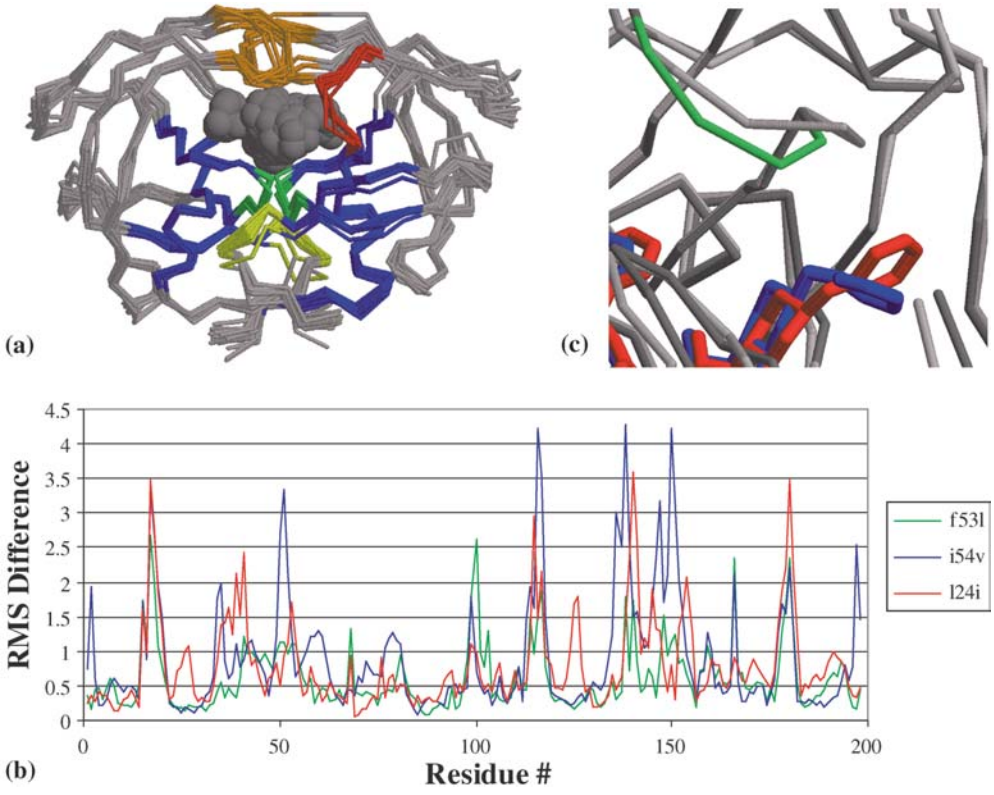

Fig. 4a–c Comparison of averaged structures. **a** The mode backbone structure is shown for all complexes in *gray* with indinavir in space-filling representation. Residues with small differences: *blue*, residues 9–13, 23–33, 83–92, 9'–13', 20'–33', 84'–97'; and *green*, residues 25–27 and 25'–27' near catalytic Asp 25/25'. Residues near indinavir with higher RMS differences: *yellow*, residues 6–8 and 6'–8'; *orange*, residues 48–53 and 48'–53'; and *red*, residues 79'–82'. **b** RMS differences on main chain atoms for mutants L24I (*red*), I54V (*blue*), and F53L (*green*) compared to WT. Residues in the dimer are numbered 1–99 and 101–199. **c** Differences near pyridyl group of indinavir. M46L (*dark gray*) versus WT (*light gray*) with 79'–82' in *green*, indinavir in *blue* for WT and *red* for M46L

Table 1 Comparison of average MD structures: overall and for regions near inhibitor

Main chain RMS differences compared to WT								
Mutant	Average (Å)	Maximum differences near indinavir						
		>2.0	>1.0	>2.0	>2.0	>1.0	>2.0	>2.0 Å
		6–8	26–27	48–53	6'–8'	26'–27'	48'–53'	79'–82'
F53L	0.78							2.3
M46I	0.87							2.4
M46L	0.87							3.0
L90M	0.91							2.9
G73S	0.92							2.9
G48V	0.92							3.0
K45I	0.94			3.2			2.0	2.3
I84V	1.01	3.6					2.1	2.3
L24I	1.02		1.1			1.8		3.5
V82A	1.05			4.3			2.2	3.2
N88D	1.06			2.6				2.6
I54V	1.23			3.4			4.2	2.2
V32I	1.30		1.4	2.2	2.7	1.1	2.0	2.6

near Arg 8, the flaps (45–55) and the loops of residues 79–82 that interact with inhibitor. All the mutants showed large changes in the positions of residues 79'–82', which indicated the variability of this loop that interacts with the pyridyl group of indinavir (Fig. 4c), in agreement with crystallographic analysis. [37] Six mutants (V32I, K45I, I54V, V82A, I84V, and N88D) showed changes in one or both of the flexible flaps. Not only the mutation of flap residues K45I and I54V, but also the binding site mutations V32I and V82A, and non-active site mutation N88D produced larger changes in the flaps. V84I showed an unusually large change in Gln 7 and V32I in Gln 7' in the

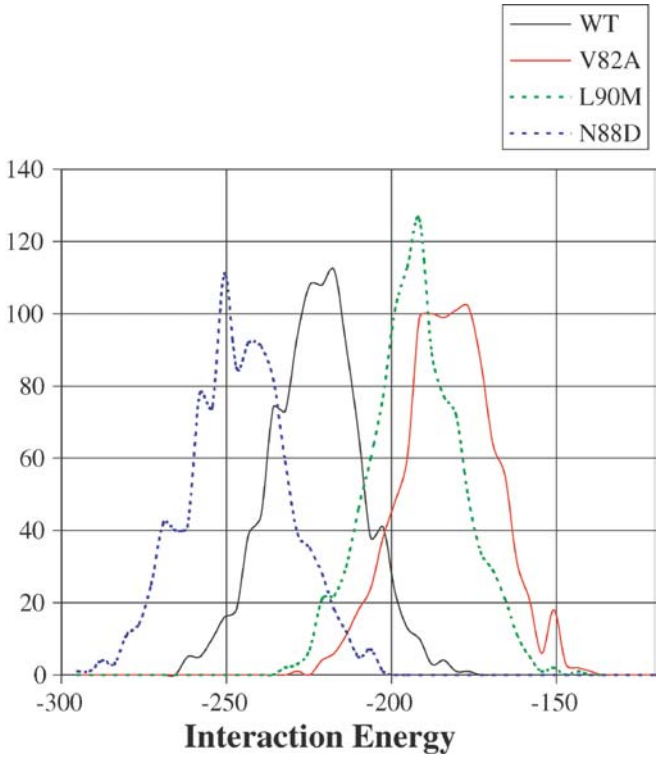

Fig. 5 Interaction energy. The protease–indinavir interaction energy is presented as a histogram calculated for each frame of the MD simulations. Values are plotted for WT (*black*), V82A (*red*), N88D (*blue*), and L90M (*green*)

surface turn next to Arg 8/8' that interacts with inhibitor. V32I showed substantial changes in almost all the sampled regions.

L24I had significant changes in the residues 26–27 of both subunits (Fig. 4b). Residue 24 does not interact directly with the indinavir; however, it is very close to the catalytic Asp 25, so changes in this region are not surprising. The only other mutant showing significant changes close to the catalytic residues was V32I, which had the largest overall RMSD compared to WT.

Estimation of protease–indinavir binding energies

The protease–indinavir interaction energy, including all the non-bonded energy terms, was calculated for each frame in the simulations. The values followed a normal distribution, as shown in Fig. 5. Therefore, the average interaction energy was calculated over the 1-ns trajectory (Table 2). The averaged interaction energy for 1,000 protease–indinavir conformations is expected to be a better estimate than the value for any individual structure. In order to validate the calculations the experimental values for differences in free energy were derived from the relative inhibition constants of wild type protease and mutants V32I, M46I, V82A and I84V taken from Gulnik et al. [12] The average interaction energy is an excellent estimate of the trends in indinavir binding to these mutants with a correlation coefficient of R=0.96. Therefore, the average interaction energy can be used to obtain a better prediction of the indinavir binding constants for the other mutants of HIV protease that are observed in drug resistant clinical isolates. The relative inhibition of the protease mutants by indinavir is predicted to be in the order listed in Table 2. The majority of mutants were predicted to be inhibited less strongly than wild type protease, as expected from their appearance in isolates resistant to indinavir. [7] Mutations of V82 and I84 are common in high level resistance to indinavir, which is in agreement with the predictions of low inhibition. [9] In contrast, strong inhibition by indinavir is predicted for the mutants K45I and N88D, consistent with their absence among the resistant mutations that arise frequently on exposure to indinavir. Overall, the average interaction energy for each mutant is consistent with the phenotypic resistance.

Table 2 Calculated protease–indinavir interaction energies. $\Delta\Delta G_{obs}$ values were calculated from inhibition data in Gulnik et al. [12]. The interaction energy was calculated as the average over the 1 ns simulation for each protease–indinavir complex

Protease complex	$\Delta\Delta G_{obs}$ (kcal mol^{-1})	Interaction energy
K45I		−25.21
N88D		−23.75
WT	0	0
I54V		19.18
F53L		23.57
G73S		27.88
M46I	0.899	29.01
V32I	1.281	29.55
L90M		29.99
G48V		31.74
M46L		33.24
I84V	1.419	36.08
L24I		39.14
V82A	1.893	39.88

Discussion

The molecular basis of HIV resistance to the clinical protease inhibitor indinavir was studied using molecular dynamics simulations of wild type protease and 13 different mutants. The mutants had substitutions of residues in different regions of the protease structure. Mutations of residues in the inhibitor binding site can directly alter the affinity for indinavir by changing specific interactions. [37] The flexible flaps are important for catalysis and inhibitor binding since they fold down to form hydrogen bond interactions with the substrate or inhibitor. [38] Mutations in the flaps can alter protein stability, catalysis and inhibition. [17, 26] The role of the distal non-active site mutations is less clear, although N88D and L90M showed reduced catalytic activity and increased or decreased stability, respectively. [26] Therefore, the simulations for wild type and mutant proteases were analyzed

for the structural variability and the interaction with indinavir.

The simulations of the solvated complexes showed structural variations along the polypeptide chain that were consistent with crystallographic data. Overall, the mutants showed a range of structural variation from 70 to 140% of the wild type protease. This variation can model the flexibility of the mutant–indinavir structures. The structural variability in the MD simulations is discussed in relation to the location of the mutation in the protease structure. Higher or lower structural variations relative to wild type protease were observed for mutants that altered residues near indinavir, in the flaps, or non-active sites regions.

Mutants V32I, V82A and I84V alter residues that have van der Waals contacts with indinavir. Mutants V82A and I84V had structural variation similar to WT, while V32I showed the highest variation. This high variation may arise because V32I was the only mutant that introduced a larger side chain next to indinavir.

Mutations K45I, M46I, M46L, G48V, F53L and I54V alter residues in the flap region that do not form van der Waals contacts with indinavir. However, the flexibility of the flaps is important for the binding of substrates and inhibitors. [38] Mutant M46I showed the lowest structural variability in the simulations, consistent with previous MD simulations suggesting that M46I reduced the flexibility of the flaps. [21, 23] Flap mutant K45I was also stable in the simulation, in agreement with its observed increased stability. [26] Flap mutants M46L and F53L showed lower variation than wild type protease. However, mutants G48V and I54V showed more structural variation in the simulations. This is consistent with the experimental observation of lower stability for G48V. [26] Therefore, the simulations for flap mutants were generally in agreement with other data. Mutations in the flap region can increase or decrease the protease flexibility, and both increased (M46I) or decreased flexibility (G48V) mutants are common in drug resistant HIV.

Mutations L24I, G73S, N88D and L90M alter residues that do not interact directly with indinavir. The MD simulations suggested that L24I and L90M decreased the structural variation, while G73S and N88D had increased variation relative to wild type protease. However, N88D and L90M showed higher and lower stability, respectively [26] in contradiction with the calculated variation. L24I showed changes in residues 26–27 near the catalytic Asp 25, which may alter catalytic activity or indinavir binding and lead to resistance. Further study is needed to better understand the effects of these non-active site mutations.

The protease affinity for indinavir was estimated from the averaged molecular mechanics interaction energy. A correlation coefficient of 0.96 was obtained with experimental inhibition constants for wild type and four mutants. Similarly high correlation was observed in a recent molecular dynamics study of HIV protease with different inhibitors. [39] This agreement was clearly improved over the values reported previously for calculations on a single protease conformation, [25] where calculations for the same mutants gave a correlation coefficient of 0.81 only after a screening correction was applied. The calculations using the average over 1 ns of molecular dynamics did not require any empirical corrections. Therefore, the trends in binding were predicted for the other mutants. A range of values was predicted for individual mutations of indinavir-binding residues, flap residues, and non-active site residues. All mutants, except K45I and N88D, were predicted to be inhibited more weakly by indinavir compared to the WT enzyme. The mutants V32I, V82A and I84V that alter residues in the indinavir-binding site were inhibited more weakly than the WT protease in the calculations and experiments. However, the six flap mutants and four distal mutants varied in the predicted relative affinity for indinavir. Flap mutants I54V and F53L were the closest to the WT. Mutant L24I near the catalytic site was predicted to be very weakly inhibited, similar to the mutants V82A and I84V, while K45I in the flap and distal N88D were predicted to be the most strongly inhibited by indinavir. The predictions were in general agreement with the occurrence of the mutations during clinical resistance to indinavir treatment. [7, 9] Therefore, this method has potential for selection of the best inhibitor for treatment of resistant HIV.

Acknowledgements This work was supported in part by the Georgia Research Alliance and the United States Public Health Service Grants GM62920 and GM065762 (to I.T.W. and R.W.H.).

References

1. Tamalet C, Pasquier C, Yahi N, Colson P, Poizot-Martin I, Lepeu G, Gallais H, Massip P, Puel J, Izopet J (2000) J Med Virol 61:181–186
2. Shafer RW, Winters MA, Palmer S, Merigan TC (1998) Ann Intern Med 128:906–911
3. Hertogs K, Bloor S, Kemp SD, Van den Eynde C, Alcorn TM, Pauwels R, van Houtte M, Staszewski S, Miller V, Larder BA (2000) AIDS 14:1203–1210
4. Vergne L, Peeters M, Mpoudi-Ngole E, Bourgeois A, Liegeois F, Toure-Kane C, Mboup S, Mulanga-Kabeya C, Saman E, Jourdan J, Reynes J, Delaporte E (2000) J Clin Microbiol 38:3919–3925
5. Condra JH, Holder DJ, Schleif WA, Blahy OM, Danovich RM, Gabryelski LJ, Graham DJ, Laird D, Quintero JC, Rhodes A, Robbins HL, Roth E, Shivaprakash M, Yang T, Chodakewitz JA, Deutsch PJ, Leavitt RY, Massari FE, Mellors JW, Squires KE, Steigbigel RT, Teppler H, Emini EA (1996) J Virol 70:8270–8276
6. Brown AJ, Korber BT, Condra JH (1999) AIDS Res Hum Retroviruses 15:247–253
7. Rhee SY, Gonzales MJ, Kantor R, Betts BJ, Ravela J, Shafer RW (2003) Nucleic Acids Res 31:298–303
8. Shafer RW, Hsu P, Patick AK, Craig C, Brendel V (1999) J Virol 73:6197–6202
9. Shafer RW (2002) Clin Microbiol Rev 15:247–277
10. Wlodawer A, Vondrasek J (1998) Annu Rev Biophys Biomol Struct 27:249–284
11. Vacca JP, Dorsey BD, Schleif WA, Levin RB, McDaniel SL, Darke PL, Zugay J, Quintero JC, Blahy OM, Roth E, Sardana VV, Schlabach AJ, Graham PI, Condra JH, Gotlib L, Hollaway MK, Lin J, Chen I-W, Vastag K, Ostovic D, Anderson PS, Emini EA, Huff JR (1994) Proc Natl Acad Sci USA 91:4096–4100

12. Gulnik SV, Suvorov LI, Liu B, Yu B, Anderson B, Mitsuya H, Erickson JW (1995) Biochem 34:9282–9287
13. Chen Z, Li Y, Schock HB, Hall D, Chen E, Kuo LC (1995) J Biol Chem 270:433–436
14. King NM, Melnick L, Prabu-Jeyabalan M, Nalivaika EA, Yang SS, Gao Y, Nie X, Zepp C, Heefner DL, Schiffer CA (2002) Protein Sci 11:418–429
15. Muzammil S, Ross P, Freire E (2003) Biochemistry 42:631–638
16. Olsen DB, Stahlhut MW, Rutkowski CA, Schock HB, van Olden AL, Kuo LC (1999) J Biol Chem 274:23699–23701
17. Ohtaka H, Schon A, Freire E (2003) Biochemistry 42:13659–13666
18. Harrison RW, Weber IT (1994) Protein Eng 7:1353–1363
19. Liu H, Müller-Plathe F, van Gusteren WF (1996) J Mol Biol 261:454–469
20. Trylska J, Grochowski P, McCammon JA (2004) Protein Sci 13:513–528
21. Collins JR, Burt SK, Erickson JW (1995) Nat Struct Biol 2:334–338
22. Scott WR, Schiffer CA (2000) Structure Fold Des 8:1259–1265
23. Piana S, Carloni P, Rothlisberger U (2002) Protein Sci 11:2393–2402
24. Wang W, Kollman PA (2001) Proc Natl Acad Sci USA 98:14937–14942
25. Weber IT, Harrison RW (1999) Protein Eng 12:469–474
26. Mahalingam B, Louis JM, Reed CC, Adomat JM, Krouse J, Wang YF, Harrison RW, Weber IT (1999) Eur J Biochem 263:238–245
27. Harrison RW (1993) J Comp Chem 14:1112–1122
28. Weber IT, Harrison RW (1996) Protein Eng 9:679–690
29. Weber IT, Harrison RW (1997) Protein Sci 6:2365–2374
30. Bagossi P, Zahuczky G, Tozser J, Weber IT, Harrison RW (1999) J Mol Model 5:143–152
31. Harrison RW (1999) J Math Chem 26:125–137
32. Harrison RW (2003) Amortized fast multipole algorithm for molecular modeling. In: Dey PP, Amin MN, Gatton TM (eds) Proceedings of the International Conference on Computer Science and its Applications. pp 77–81
33. Jones TA, Zou JY, Cowan SW, Kjeldgaard M (1991) Acta Crystallogr A47:110–119
34. Sayle RA, Milner-White JE (1995) Trends Biochem Sci 20:374–376
35. Zoete V, Michielin O, Karplus M (2002) J Mol Biol 315:21–52
36. Chen Z, Li Y, Chen E, Hall DL, Darke PL, Culberson C, Shafer JA, Kuo LC (1994) J Biol Chem 269:26344–26348
37. Munshi S, Chen Z, Yan Y, Li Y, Olsen DB, Schock HB, Galvin BB, Dorsey B, Kuo LC (2000) Acta Crystallogr D56:381–388
38. Gustchina A, Weber IT (1990) FEBS Lett 269:269–272
39. Jenwitheesuk E, Samudrala R (2003) BMC Struct Biol 3:2